Microporous and Mesoporous Materials 191 (2014) 1–9

Contents lists available at ScienceDirect

Microporous and Mesoporous Materials

journal homepage: www.elsevier.com/locate/micromeso

Synthesis, characterization and application of a hexagonal mesoporous silica for pesticide removal from aqueous solution

Maximiliano Brigante *, Marcelo Avena

INQUISUR, Departamento de Química, Universidad Nacional del Sur, Av. Alem 1253, 8000 Bahía Blanca, Argentina

ARTICLE INFO

Article history:
Received 23 December 2013
Received in revised form 7 February 2014
Accepted 21 February 2014
Available online 3 March 2014

Keywords:
MCM-41
Solid–water interface
Paraquat adsorption
Electrostatic interactions
Surface complexes

ABSTRACT

A hexagonal mesoporous silica (SiO_2) was hydrothermally synthesized in alkaline media by using mixed cationic cetyltrimethylammonium tosylate-non-ionic Pluronic F68 surfactants as template. After characterization by commonly used techniques, the solid was evaluated as adsorbent for the remotion of dicationic herbicide paraquat (PQ^{2+}). The adsorption of the PQ^{2+} on SiO_2 has been studied in batch experiments by performing adsorption isotherms under different conditions of pH, supporting electrolyte concentration, and temperature. Adsorption kinetic on the studied material has also been carried out and discussed. The adsorption of PQ^{2+} on the studied material is strongly dependent on pH, increasing as pH increases. The adsorption seems to take place by direct binding of the cationic herbicide to SiO_2 active sites (e.g. surface and/or inside the mesopores) through electrostatic interactions and outer-sphere (or ionic pair) complexes formations, as deduce from adsorption experiments at several ionic strengths and temperatures. The analysis of thermodynamic parameters suggests that the adsorption of PQ^{2+} on the studied solid is exothermic and spontaneous in nature. Even after four regeneration cycles through acid washing, the mesoporous material has still a removal efficiency of ca. 75%, showing a promising application for the treatment of wastewater containing paraquat ions.

1. Introduction

Use of agrochemicals constitutes an unpleasant task but absolutely necessary to tackle the multiple kind of adverse events that can irremediably damage the quality of various crops. On the other hand, serious health effects may be promoted due to pesticide discharges from manufacturing plants, surface runoff, leaching accidental spills and other sources [1]. In fact, there are several papers that report pesticide concentrations in waste and surface waters higher than pollution threshold limit [2]. Harmfulness of agrochemicals is further enhanced by their mobility and persistence in the aqueous media [3].

Among the numerous agrochemicals in use today, the herbicide paraquat (1,1′-dimethyl-4,4′-dipyridinium chloride) is the most widely used in the world, although it has been forbidden in the European Union since 2007. Its popularity is related to its physical and chemical properties (e.g. high solubility in water, low vapor pressure and high binding potential) and to its quick and non-selective action to kill green plant tissue upon contact [4,5]. Paraquat (PQ^{2+}), also known under the name of methyl viologen, kills green plants by inhibiting the conversion of nicotinamide adenine dinucleotide phosphate (NADP) to its hydrogen form NADPH during photosynthesis [6]. Additionally, some studies proved that this compound is one of the few herbicides capable of controlling the growth of weeds that became resistant as a result of over-use of non-selective glyphosate herbicides [7]. However, it is known that this herbicide is one of the most toxic poisons if deliberately or accidentally ingested. PQ^{2+} has toxic effects on the lungs, livers, and kidneys of mammals [6]. In recent years, investigations on PQ^{2+} toxicity have suggested that this herbicide might be an environmental factor contributing to a neurodegenerative disorder, such as Parkinson's disease [8]. World Health Organization (WHO) has reported this herbicide as the "major suicide agent" which killed several thousands of people in the past few years due to its acute toxicity, its relative cheap price and its lack of a known effective antidote [9]. Therefore, and as it has not yet been established an effective therapy for acute PQ^{2+} poisoning, it is of great interest the development of an effective adsorbent as antidote or filter for the removal of herbicides from poisoned circulation system or contaminated environment, mainly on solids with high surface area, pore size and catalytic activity.

Since 1990, mesoporous silica and silica-based materials have attracted considerable attention because of their high surface area (>200 $m^2\ g^{-1}$), ordered pore distribution, narrow pore size

* Corresponding author. Tel.: +54 291 4595101x3593.
E-mail address: brigante@uns.edu.ar (M. Brigante).

http://dx.doi.org/10.1016/j.micromeso.2014.02.035
1387-1811/

distribution (2–>10 nm, higher than zeolites), high thermal stability and easy regeneration and reusability in comparison with several soils and soil components [10,11]. Due to these properties, they are ideal base materials for catalyst, catalyst support and adsorbent as well as template for other materials. Particularly, silica materials with two-dimensional (2D) hexagonal array of uniform cylindrical mesopores (*p6mm* space group), like MCM-41, SBA-3 or SBA-15, have attracted considerable attention for possible application as adsorbents because their mesostructures provide the pore size required for the adsorption of large molecules of gas and liquid [12]. MCM-41 and SBA-3 are commonly synthesized by using a cationic surfactant of the family of quaternary ammonium salts as template (i.e., CTAX, where CTA^+ is the cetyltrimehtylammonium ion and X^- is the Br^- or Cl^- counterion) [11, 13]. SBA-15, on the contrary, is frequently synthesized by using the non-ionic triblock poly(oxyethylene)–poly(oxypropylene)–poly(oxyethylene) copolymer Pluronic P123 [12]. Recently, several researchers have reported the formation of well-ordered and high thermally-stable mesostructures by using the dual template system CTAX-Pluronic, although the formation of either MCM- or SBA-type materials is strongly related to the experimental synthesis conditions, such as pH, temperature, surfactant concentration, $CTAT^+$/Pluronic molar ratio, type of X^-, calcination temperature, etc. [14,15].

There are several papers in literature related to the adsorption of PQ^{2+} on porous materials, especially concerning zeolites. On the one hand, Ibrahim and Jbara [16] reported that the adsorption of PQ^{2+} on a natural zeolitic material such as phillipsite–faujasite stuff strongly enhances when the adsorbent is thermally activated and/or modified with monovalent cations such as K^+ and Na^+. Cation exchange was reported to play a key role on the adsorption process. Similar mechanism was reported by Zhang et al. [17] and later by Rongchapo et al. [18] on the adsorption of the pesticide on a surface-modified zeolite Y. On the other hand, Shieh et al. [19] showed that the adsorption of PQ^{2+} on amino acid-functionalized SBA-15 strongly depends on the time and pH of the solution, but not on the temperature. The adsorption mechanism was related to π–π stacking interactions between the adsorbent and the adsorbate.

The aim of this article is to present a study of PQ^{2+} adsorption on a hexagonal mesoporous silica. The adsorbent was hydrothermally synthesized in alkaline media by using a mixed-surfactant template composed by the cationic surfactant cetyltrimethylammonium tosylate and the amphiphilic copolymer Pluronic F68. On the one hand, and as far as we know, there is no information in the literature on the silica synthesis by using this mixture since we have introduced it in 2012 [20]. On the other hand, the adsorption data obtained at a variety of pH, ionic strength, temperature, and reuse cycles are used to gain insights into the mechanisms that govern the adsorption process and into the factors that promote or prevent it. The obtained results will also serve as a basis for further synthesis of new materials for pollution control.

2. Materials and methods

2.1. Chemicals

Paraquat dichloride (MW = 257.16 g mol^{-1}), cetyltrimethylammonium *p*-toluene sulfonate or tosylate (CTAT, MW = 455.7 g mol^{-1}), Pluronic F68 ($PEO_{76}PPO_{29}PEO_{76}$, MW = 8400 g mol^{-1}, and PEO and PPO being the poly(oxyethylene) and the poly(oxypropylene) chain units, respectively) and tetraethyl orthosilicate (TEOS, 99%) were purchased from Aldrich. Potassium hydroxide, potassium chloride, potassium nitrate, nitric acid, hydrochloric acid, sodium acetate, acetic acid, sodium carbonate, sodium hydroxide, sodium hydrogen carbonate, disodium phosphate anhydrous, and monosodium phosphate anhydrous were obtained from Anedra.

All chemicals were of analytical grade and used as received. Double distilled water was used for the preparation of solutions.

2.2. Synthesis and characterization of mesoporous silica

Mesoporous silica (SiO_2) was prepared using a procedure similar to that described in an earlier work [20]. Briefly, 11.6 mL of TEOS were mixed with 2 mL of water and stirred in an autoclave flask for 10 min at 500 rpm. At the same time, 38 mL of Pluronic F68-CTAT mixed solution were prepared with a 1:3 M ratio by adding the desired amount of surfactants to water. This mixture was stirred in a conical flask at 35 °C to form a transparent template solution and then it was left at room temperature. To obtain the mesoporous material, 20 mL of a 1.43 M NaOH solution were added drop by drop to the TEOS solution under stirring and 2 min later the surfactant solution was incorporated. The final pH of the mixture was around 11.8. The resulting gel, whose composition was 1 TEOS:0.53 NaOH:0.011 CTAT:0.0037 F68, was stirred for 5 min and then left for 48 h in an autoclave at 100 °C. After this, the gel was filtered and washed with distilled water and dried at room temperature. Finally, it was calcined in an air flux by increasing the temperature from room temperature to 540 °C with a heating rate of 2 °C min^{-1}, and holding for 7 h at 540 °C.

The synthesized material was characterized by the techniques usually employed in porous materials, such as scanning and transmission electron microscopy (SEM and TEM); XRD; FT-IR spectroscopy; electrophoretic mobility measurements; and the N_2-BET method for surface area, pore volume and pore diameter determination. SEM was performed using an EVO 40-XVP microscope. The sample was prepared on graphite stubs and coated with a ca. 300 Å gold layer in a PELCO 91000 sputter coater. TEM was performed using a JEOL 100 CX II transmission electron microscope, operated at 100 kV with magnification of 450,000×. Observations were made in a bright field. The powdered SiO_2 was placed on 2000 mesh copper supports. XRD patterns were obtained via a Philips PW 1710 diffractometer with CuKα radiation (λ = 1.5406 Å) and graphite monochromator operated at 45 kV, 30 mA and 25 °C; the angle step and counting time were 0.02°(2θ) and 1 s, respectively. The electrophoretic mobility of SiO_2 was measured with a Zetasizer Nano Series instrument (Malvern Instruments Ltd.) at room temperature, and the Zeta potential was calculated using the Smoluchowski equation [21]. Stock suspensions containing 0.1 g L^{-1} of solid in 10^{-2} M KNO_3 were used for the measurements. The pH of the suspensions was adjusted to the desire value by adding small volumes of HNO_3 or KOH solutions. The N_2 adsorption isotherms at 77.6 K were measured with a Quantachrome Nova 1200e instrument. The sample was degassed at 373 K for 720 min at a pressure of 1×10^{-4} Pa. FT-IR experiments were recorded in a Nicolet FT-IR Nexus 470 Spectrophotometer. To avoid co-adsorbed water the sample was dried under vacuum until constant weight and then it was diluted with KBr powder before the FT-IR spectrum was recorded.

2.3. Adsorption experiments

Adsorption experiments (in darkness to avoid photodegradation) were obtained with a batch equilibration procedure using 15 mL polypropylene centrifuge tubes covered with polypropylene caps immersed in a thermostatic shaker bath. Before starting the experiment, a stock PQ^{2+} solution (2×10^{-3} M) was prepared by adding the corresponding solid to buffer solutions. The pHs investigated were 4.4 (0.1 M acetate/acetic acid), 7.0 (0.1 M $HPO_4^{2-}/H_2PO_4^-$), and 9.5 (0.1 M CO_3^{2-}/HCO_3^-). 50 mg of mesoporous material were introduced into the tubes and mixed with varying

quantities of PQ^{2+} and KCl (used as supporting electrolyte) solutions. The range of initial PQ^{2+} concentration was 5×10^{-6}–1×10^{-3} M, and the final volume was 8 mL. The stirring rate was kept constant at 90 rpm. At different reaction times, the particles were separated from the supernatant by centrifugation at 4000 rpm during 2 min and the supernatant was immediately analyzed to quantify the concentration of adsorbed PQ^{2+}. After the quantification (see below), that took around 30 s, the supernatant was reintroduced into the tube. This procedure (separation, quantification of PQ^{2+} and reintroduction of the supernatant into the reaction tube) was repeated during several hours in order to achieve complete adsorption of the pesticide or to gather enough data points. The last data point obtained in these experiments was assumed to represent equilibrium conditions. Adsorbed PQ^{2+} was calculated from the difference between the initial PQ^{2+} concentration and the concentration of the pesticide that remained in the supernatant solution. In most experiments supporting electrolyte was not used and the working temperature was 25 °C (except when effects of KCl concentration and temperature were investigated).

Quantification of PQ^{2+} was performed by UV–VIS spectroscopy at 257 nm using an Agilent 8453 UV–VIS diode array spectrophotometer equipped with a Hellma 1 cm quartz cell. The supernatant of the withdrawn aliquot was placed into the cell and the spectrum was recorded in the 200–900 nm wavelength range. Calibration curves at the working pH were also constructed with several PQ^{2+} solutions having concentration that ranged between 2.00×10^{-6} and 1.50×10^{-4} μM. Very good linearity was found in all cases ($r^2 > 0.998$).

The adsorption kinetic is traditionally described following the expressions of the pseudo-first and the pseudo-second order equations originally given by Lagergren, which are special cases for the general Langmuir rate equation [22]. The pseudo-second order model, described by Eq. (1), was used here and in most solid/solution interaction studies [23]:

$$\frac{t}{q_t} = \frac{1}{k_{2,s} q_e^2} + \frac{1}{q_e} t \tag{1}$$

where $k_{2,s}$ is the pseudo-second-order rate constant (g μmol^{-1} min^{-1}); and q_e and q_t (μmol g^{-1}) denote the amount of pesticide adsorbed at equilibrium and at the reaction time t, respectively. The fitting validity of this model is traditionally checked by the linear plots of t/q_t versus t. The slope and intercept of the obtained straight line provide the respective kinetic constant and the q_e parameter.

Despite the Lagergren kinetic equations have been used in a great deal of adsorption kinetic works, this model cannot give interaction mechanisms, so another model was also used to test pesticide adsorption on the studied materials. An intraparticle diffusion model (Morris–Weber model), described by Eq. (2), was examined [23]:

$$q_t = k_{int} t^{0.5} + I \tag{2}$$

where k_{int} is the intraparticle diffusion rate constant and I is the intercept. I is also an indicator about the thickness of boundary layer, i.e., the larger the intercept, the greater the boundary layer effect. According to the model, if intraparticle diffusion is the rate-limiting step of the whole adsorption process, the plot of q_t versus $t^{0.5}$ yields a straight line passing through the origin. Otherwise, some other mechanisms are possibly involved along with intraparticle diffusion.

The adsorption isotherms were fitted using a Langmuir equation, which was commonly used in the adsorption of pesticides on several adsorbent systems [24,25]. The linear form of this equation is displayed as follows:

$$\frac{1}{PQ_{ads}^{2+}} = \frac{1}{q_{mon}} + \frac{1}{q_{mon} K_L PQ_{eq}^{2+}} \tag{3}$$

where PQ_{ads}^{2+} is the adsorbed amount of PQ^{2+} (μmol g^{-1}), PQ_{eq}^{2+} is the equilibrium concentration of MC in the supernatant (μM), q_{mon} is the maximum amount of pesticide adsorbed (μmol g^{-1}) corresponding to complete coverage on the surface, and K_L is the Langmuir constant (μM^{-1}). From the linearized form of Eq. (3), q_{mon}, K_L, and the correlation coefficient, r^2, can be calculated.

2.4. Regeneration and reuse of the adsorbent

In order to evaluate both the possibility of regeneration of the adsorbent and its reusability, 40 ml of a 2×10^{-4} M PQ^{2+} solution (previously prepared in carbonate buffer, pH 9.5) were mixed with 250 mg of mesoporous material. The suspension was then stirred in a 50 mL polypropylene centrifuge tube covered with a polypropylene cap for 12 h at pH 9.5 and 25 °C. After that, the supernatant was extracted by centrifugation for quantifying the amount of adsorbed PQ^{2+} and the solid was successively washed with a 0.25 M HCl solution with vigorous stirring up to complete desorption of the pesticide (or up to confirm the no appearance of 257 nm band of PQ^{2+} by UV–VIS spectroscopy). Then, the regenerated adsorbent was thoroughly washed with double-distilled water until a neutral pH was obtained. To be reused in the next cycle of adsorption experiments, the regenerated material was then dried at 60 °C overnight and suspended with the PQ^{2+} solution (2×10^{-4} M). The adsorption–desorption cycle was repeated up to four times. For comparison, similar experiments were carried out without using the HCl solution as extracting agent, i.e., the solid with the pesticide adsorbed was sequentially washed with double-distilled water. All experiments were carried out without using supporting electrolyte solutions.

3. Results and discussion

3.1. General characteristics of the synthesized material

The morphology of the studied sample, whose particles have a characteristic white coloration, was investigated by SEM and TEM techniques and the respective micrographs are presented in Fig. 1. According to the SEM images, SiO_2 consists of agglomerates of polydisperse plate-like particles whose average size is around of 1.5 μm. At higher magnifications, as shown in Fig. 1b, the material has a sandy granular aspect. At very high magnification (Figs. 1c and d), the sandy texture shows regular mesopores, having a pore diameter and pore-wall thickness of 1.94 nm and 1.47 nm, respectively.

On the one hand, it is known that the hydrothermal synthesis of mesoporous silicas in alkaline media at middle-high temperatures by using CTAT as template (CTAT/SiO_2 molar ratio 0.09:1) produces MCM-41 type materials with highly 2D hexagonal mesostructure and thick pore walls [26]. The formation mechanism is related to Columbic interactions among negative-charged silica species (I^-), due to the depronation of silanol groups, and the cationic surfactant (S^+) [26]. Additionally, the authors reported a structure transformation from MCM-41 to MCM-48 type silica (3D cubic mesostructure with *la3d* symmetry) by decreasing the synthesis temperature [27]. The formation of the cubic framework was also attributed to the retention of tosylate counteranions in the interface between surfactant and silicate [27]. A material with a structure of the type SBA-3 is not suggested to be formed here due to it is commonly synthesized at acidic pH [13]. On the other hand, it is also well-known that the synthesis of mesoporous silicas by using non-ionic surfactants as Pluronics with long hydrophilic PEO chains (e.g. Pluronics F127, F108, F88 and F68) yields SBA-16 type

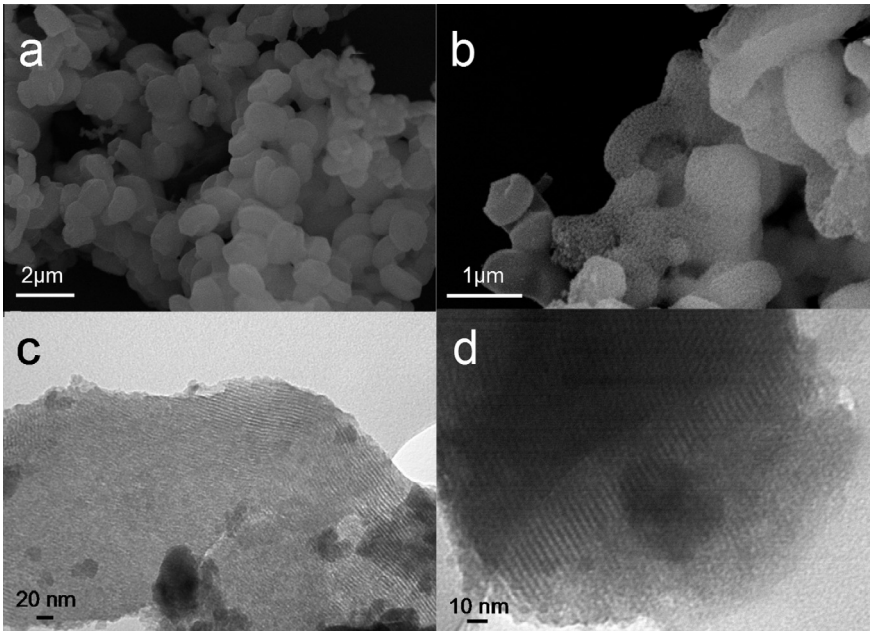

Fig. 1. Electronic micrographs of the synthesized SiO_2: (a) SEM, 20,000×; (b) SEM, 50,000×; (c) TEM, 270,000; and (d) TEM, 450,000×.

materials with 3D cubic structure (*Im3m* symmetry) [28,29]. If the PEO chain of the copolymer is short, like Pluronic P123, the 2D hexagonal mesostructure is formed [29]. The proposed formation mechanism using any Pluronics involves three stages: (i) silica coating of the surfactant micelles and decreasing of the zeta potential; (ii) formation of micrometer-sized "liquid particles" by aggregation and fusion of the composite colloids, related to silica coated micelles and (iii) solidification of the "liquid particles" and transformation into the final mesoporous silica composition [29]. In alkaline media, the non-ionic surfactant molecules interact with I^- species through an electrostatic assembly $N^0H^+I^-$, where N^0H^+ is the surfactant hydrogen bonded to a hydronium ion [30]. Since the SiO_2 produced here was synthesized in strong alkaline media (pH 11.8), at middle-high temperatures (100 °C) and by using both cationic and non-ionic surfactants (this last with long PEO chains), either of the two frameworks (i.e., hexagonal or cubic) could be formed in the solid.

Taking into account the mentioned above, two questions arise: whether the presence of two surfactants, i.e., CTAT + Pluronic F68, modify (or not) the morphology and pore structure of SiO_2 in comparison with the single surfactant and which of the two tensioactives play the key role in those parameters. Chen et al. [14] reported that in the double template system Pluronic F127-cetyltrimethylammonium bromide (CTAB) at alkaline pH (F127/CTAB molar ratio = 0.10) the cationic surfactant (i.e., CTA^+ ions) contributes to the pore structure of SiO_2 while non-ionic surfactant influences the particle size and the pore structure integrity. The proposed mechanism involves the self-assembly of negatively charged silicates (I^-) and CTA^+ micelles (S^+) to form the hexagonal structure regardless of the presence of the non-ionic species, which then surround the hexagonally ordered silica-CTA composites due to a weak interaction between ionic and non-ionic hydrophilic groups. Thus, the presence of F127 micelles covering the nanoparticles suppressed the grain growth and stabilized the ordered mesostructures [14]. On the contrary, Almeida et al. [15] reported that the inclusion of CTAB in the TEOS-Pluronic F127 system at acidic pH (F127/CTA^+ molar ratio = 0.25) changes the morphology of the material, i.e., from plate-like to dodecahedral type particles, although the symmetry was not changed from cubic SBA-16. Qi et al. [31] suggested a complex pathway in the CTAB-Pluronic F127-TEOS system at acidic pH that involves both $S^+X^-I^+$ and (N^0H^+)(X^-I^+) assemblies (X^- being the cationic surfactant counterion) at the interface of mixed micelles. However, the mentioned mechanism could change at alkaline pH due to the formation of I^- species by deprotonation of silanol groups. In order to predict if the symmetry is of the type SBA-16 or MCM-41, the pore wall thickness is other of the parameters commonly used for these purposes. For MCM-41, the pore wall thickness varies between 0.8 and 2.5 nm while SBA-16 exhibits values of 3.2 nm or higher [10,15,27]. As well shown in Fig. 1, the mesoporous material synthesized here has a pore wall thickness of 1.47 nm, which is close to a material with a *p6mm* symmetry.

The results obtained by XRD, nitrogen sorption isotherms, FT-IR spectroscopy and electrophoretic mobility of calcined sample are shown in Figs. 2a–d, respectively. In the range of 2-theta between 1.6° and 10° (inset of Fig. 2a), the solid shows three easily distinguished diffraction peaks, (100), (110), and (200), which ascribe to a highly ordered 2D hexagonal packing of MCM-41 silica [11]. The values corresponding to *d*-spacing of the 100 facet, d_{100}, and to its unit cell parameter, a_0, are 4.05 and 4.68 nm, respectively. At higher angles, SiO_2 shows a XRD pattern typical of amorphous materials, which is also characteristic of mesoporous silicas [32]. The porous structure of SiO_2 is stable under our synthesis conditions and it does not collapse during calcination at 540 °C resulting in the transformation to the cristobalite phase, as observed by Gu et al. [33]. The nitrogen sorption isotherms of SiO_2 are typical type IV isotherms with a sharp increase in volume of nitrogen adsorbed at intermediate P/P_0 which is associated with capillary condensation in mesostructured channels of the solid. Such adsorption behavior is typical of the mesoporous materials with uniform pore size and narrow pore size distribution [20]. The hysteresis loop is a type H3 which is typical of plate-like particles giving rise to slit-shaped mesopores [16]. Fig. 2b also shows that this loop is nearly reversible owing to a relatively small mesopore size (<3 nm) [34], in agreement with TEM observations. In fact, the pore radii were sharply distributed in a narrow range located at 0.97 nm, as shown from BJH adsorption pore size distribution (inset of Fig. 2b). If the data from N_2 desorption step were used, the pore size distribution

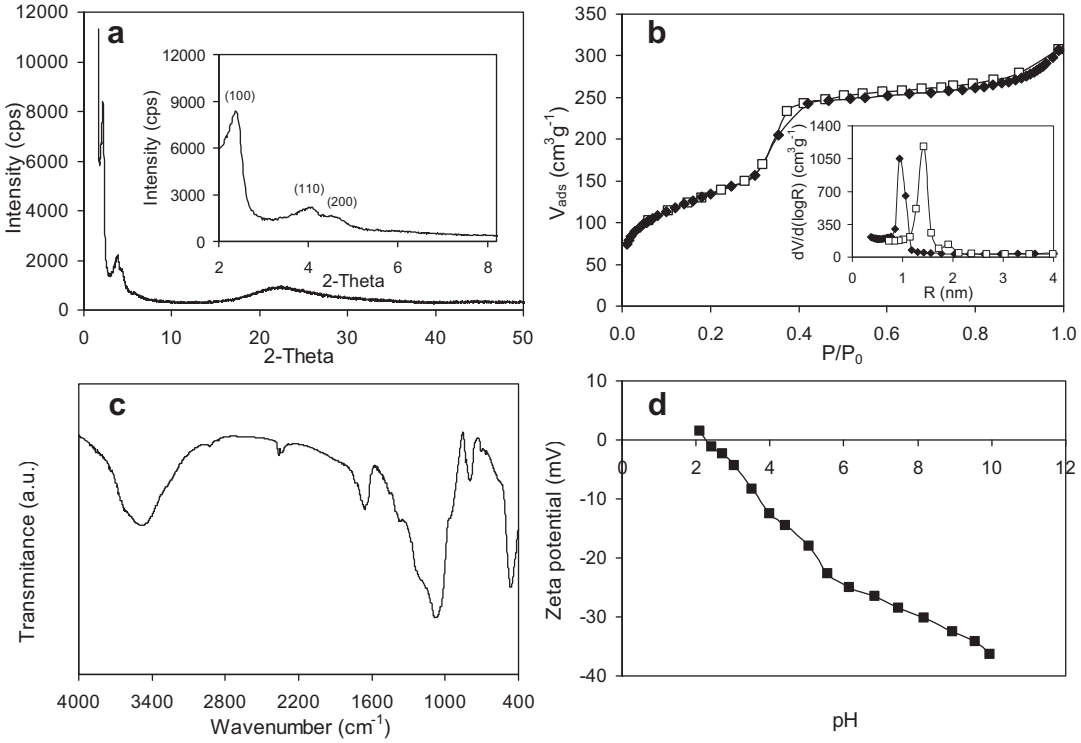

Fig. 2. Characterization of studied sample by: (a) XRD; (b) N_2 sorption isotherms, where the inset shows the pore radius distribution obtained from adsorption (close diamonds) and desorption (open squares) data; (c) infrared spectroscopy; and (d) electrophoretic mobility measurements as a function of pH in a 10^{-3} M KNO_3 solution. All studied were performed by using the solid in the calcined form.

has also a narrow shape with a maximum radius centered at 1.42 nm. This average pore width is also close to microporosity or small mesopores. The uniformity on the pore size is mainly attributed to the use of the F68 triblock copolymer in the material synthesis [20]. The calculated BET surface area (A_{BET}) and average pore volume were 468 $m^2\,g^{-1}$ and 0.474 $cm^3\,g^{-1}$, respectively.

Ravikovitch et al. [35], on the contrary, reported that the BJH model can give incorrect results when the material has pore sizes in the order of 2 nm or lower. Moreover, the authors also suggested that the application of theoretical methods, such as nonlocal density functional theory (NLDFT) and Monte Carlo simulations, could act as powerful tools to predict the pore size of this kind of materials. This is due to the fact that these models provide a more accurate structure of a fluid confined to narrow pores. However, when the BJH and NLDFT were compared a difference of around 1 nm in the calculated pore diameter was obtained [35]. The authors state that this may be a consequence of (a) the underestimation of the average pore size with the BJH model when the material has pore sizes close to microporosity, and/or (b) the assumption of the solid with ideal cylindrical pore structure with the NLDFT model.

The pore diameter (D_p) and the pore wall thickness (W_t) can be also calculated from XRD and BET surface area data as follows:

$$D_p = c d_{100}\left(\frac{\rho V_p}{1+\rho V_p}\right)^{0.5}, \quad (4)$$

$$W_t = \frac{2}{\sqrt{3}} d_{100} - \frac{D_p}{1.05}, \quad (5)$$

where c is a constant characteristic of the pore geometry, V_p is the pore volume and ρ is the pore wall density (assumed to be 2.2 $cm^3\,g^{-1}$ for silicas with amorphous pore walls) [36]. The constant c is equal to 1.213 for circular as well as hexagonal pores, but in the latter case, D_p is defined as the diameter of a circle of the same area as the hexagonal pore cross section [36]. W_t was calculated under assumption of the hexagonal pore geometry, as observed from TEM images. The values of D_p and W_t were 3.51 and 1.33 nm, respectively. The differences in D_p obtained from Eq. (4) and that obtained from BJH method are attributed to the fact that XRD assumes an ideal hexagonal unit cell [35]. The calculated W_t is similar to that estimated from TEM studies confirming that the pore wall in MCM-41 practically does not depend on the pore size [35].

The most important features of the FT-IR spectra of SiO_2 are: a broad band centered at 3504 cm^{-1} associated to OH stretching of surface hydroxyls bound to silicon (Si–OH); a peak at 1654 cm^{-1} due to the OH bending mode of water molecules; a broad peak located at 1078 cm^{-1} with shoulders at 1195 and 1364 cm^{-1} which are attributed to asymmetric Si–O–Si vibrations; a peak centered at 795 cm^{-1} due to symmetric Si–O–Si vibrations; and peaks at 962 and 465 cm^{-1} assigned for Si–O–Si bending modes [37]. Finally, the Zeta potential versus pH data show that the mesoporous material has an isoelectric point (IEP) of 2.2, which is in agreement with those reported in the literature [[38], and references therein].

3.2. PQ^{2+} adsorption studies

Adsorption kinetics of PQ^{2+} on SiO_2 as a function of pH is shown in Fig. 3. The adsorption is very fast between $t = 0$ and $t = 5$ min in almost all experiments (Fig. 3a). It is so fast that no data point could be measured in this period with our experimental set up. At $t > 5$ min the adsorption takes place at a much slower and measurable rate, and at around 50 min equilibrium seems to be reached in all cases. The very fast process can be related to an adsorption reaction where the PQ^{2+} ions present in the aqueous solution directly bind silica surface groups [39]. Besides, the negatively charged silanol groups in the pores are assumed to be

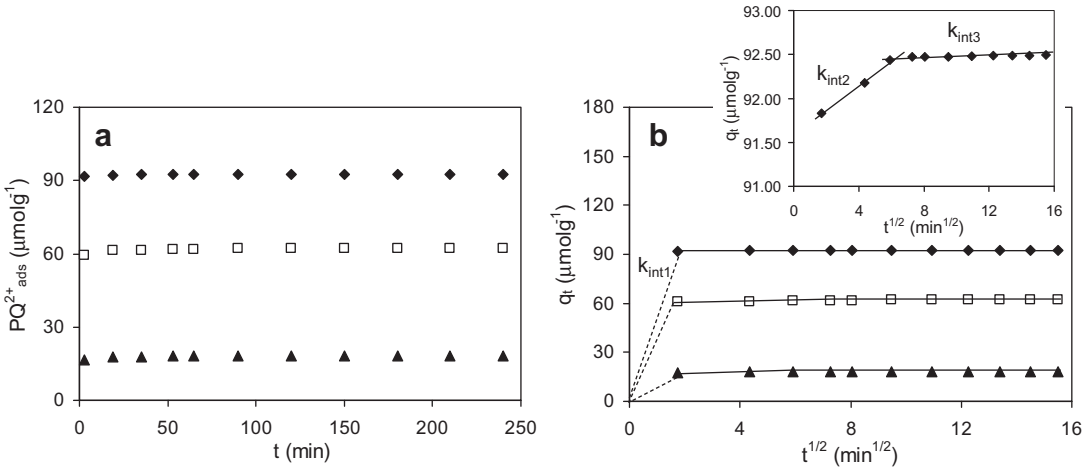

Fig. 3. Effect of pH on the adsorption kinetics of PQ^{2+} on SiO_2 at 25 °C: (a) adsorption rate, and (b) q_t versus $t^{0.5}$ for intraparticle diffusion model. pH values: diamonds, pH 9.5; squares, pH 7.0; and triangles, pH 4.4. The inset of (b) shows the magnification of the intraparticle diffusion model performed at pH 9.5.

accessible for binding the pesticide. However, there is no consensus thus far regarding the type of reaction taking place in the slow process. This step can be attributed to the fact that: (a) the adsorption equilibrium is reached, where both the adsorption and desorption rates are similar and/or, (b) several possible mechanisms can occur including intraparticle diffusion or diffusion into pores, surface binding heterogeneity and others [40]. However, whatever the process is, it is clear that this second step is much slower than the other one and takes minutes (or even hours) for completion. Fig. 4a also shows that the adsorption is strongly dependent on the pH, i.e., it is relatively high at low pH and decreases significantly. All data were fitted well to the pseudo-second-order kinetic model with $r^2 = 1$, as shown in Table 1.

It is interesting to remark that the good-on-fit of Eq. (1) is strongly related to the initial concentration of adsorbate. Azizian [22] reveals, based on the derivation of both pseudo-first and pseudo-second order models, that the sorption process obeys the first at high initial concentrations of solute, while it obeys the second at lower initial concentrations. In fact, the application of the pseudo-first kinetic model to our results (data not shown) yields r^2 values of 0.79–0.90 at all studied pH. The author also shows that the obtained rate constants are combinations of adsorption and desorption rate constants and also initial concentration of solute [22]. However, and as mentioned above, none of the mentioned kinetics models give information about the adsorption mechanism.

If the Weber–Morris model is applied to our results, as shown in Fig. 3b, at least three linear sections with different slopes are obtained. The multilinearity indicates that three (or more) steps occur in the sorption process. The first (dotted line between $t = 0$ and $t = 5$) is commonly attributed to the boundary layer diffusion or instantaneous adsorption on the external surface and/or inside the mesopores; this step represents almost the 95% of pesticide adsorbed. The second is attributed to the gradual or slow adsorption stage where intra-particle diffusion is the rate limiting step; this step was also ascribed to the diffusion in mesopores [41]. The third is related to the decrease of the intra-particle diffusion rate due to the fact that the adsorption equilibrium is reached [41]. The last step is also attributed to the diffusion in micropores [42]. The results suggest, therefore, that the mechanism of PQ^{2+} adsorption over the surface of the studied solids is complex and both the adsorption on external surface (and/or inside the pores) as well as intraparticle diffusion contribute to the actual adsorption process. Table 1 also shows the k_{int} values which are obtained from the slopes of Fig. 3b. It is important to be noted that the k_{int1} values were estimated from the slope of the straight lines plotted between the origin and $t = 5$ min.

The effect of pH on the adsorption can be better observed in the respective isotherms, as shown in Fig. 4. The shape of the curves is similar to the shape of the isotherms reported in a previous paper for the adsorption of PQ^{2+} on goethite modified with a humic acid

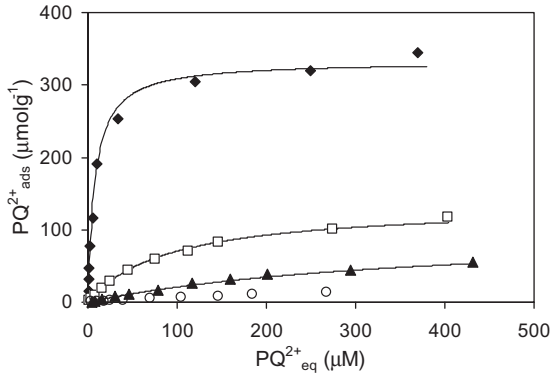

Fig. 4. Effect of pH on the adsorption of PQ^{2+} on SiO_2 at 25 °C. pH values: diamonds, pH 9.5; squares, pH 7.0; and triangles, pH 4.4. Circles show the adsorption of the herbicide on SiO_2 synthesized in alkaline media by using CTAB as template. Lines show predictions of Eq. (3).

Table 1
Kinetic adsorption parameters for PQ^{2+} adsorption on SiO_2.

pH	Pseudo-second-order model			Intraparticle difussion model					
	q_e (μmol g^{-1})	$k_{2,s} \times 10^3$ (g μmol^{-1} min^{-1})	r^2	k_{int1} (μmol g^{-1} t$^{-1/2}$)	r^2	k_{int2} (μmol g^{-1} t$^{-1/2}$)	r^2	k_{int3} (μmol g^{-1} t$^{-1/2}$)	r^2
4.4	18.21	81.38	1.00	10.199	1.00	0.061	0.99	0.021	0.86
7.0	62.11	108.00	1.00	35.235	1.00	0.138	0.99	0.025	0.98
9.5	92.59	291.60	1.00	53.020	1.00	0.143	1.00	0.003	0.99

[24] and those reported by Tsai et al. [25], Rytwo et al. [43] and Iglesias et al. [44] for the adsorption of the pesticide on diatomaceous earth, montmorillonite and humic substances, respectively. As expected, the adsorption is relatively high at pH 9.5 and decreases significantly at pH 7 and 4.4 indicating that the affinity of PQ^{2+} for SiO_2 is higher at high pH. From the data of zeta potential versus pH (Fig. 3d), it is clear that the surface of SiO_2 at the experimental conditions (i.e., pH > 4.4) should exhibit negative charges mainly due to the variable charge from pH dependent surface hydroxyl sites [45]. Thus, it is noted that with the increase of pH the adsorbed amount of cationic paraquat increases in response to the increasing number of negatively charged sites that are available due to the loss of H^+ from the surface [45]. Fig. 4 also shows that the adsorption of PQ^{2+} on SiO_2 strongly depends on the experimental conditions which the adsorbent was synthesized. In fact, the q_{mon} value of the SiO_2 synthesized in this work is 25-times higher than those obtained in a previous paper for the adsorption of the pesticide on silica synthesized in alkaline media by using the cationic surfactant CTAB as template [39]. Moreover, the adsorption on that material was only detected at pH 9.5. This reveals that the synthesis conditions, e.g. pH and type and concentration of surfactant/s used as template play an important role on the morphology (i.e., the A_{BET} and V_p of SiO_2-CTAT and SiO_2-CTAB were 480.6 $m^2\ g^{-1}$ and 0.47 $cm^3\ g^{-1}$, and 238.6 $m^2\ g^{-1}$ and 0.41 $cm^3\ g^{-1}$, respectively) and on the reactivity of mesoporous silicas.

The direct binding between paraquat and silica can be visualized comparing the FT-IR spectra of SiO_2, PQ^{2+} and PQ^{2+} adsorbed on SiO_2 at pH 9.5 such as shown in Fig. 5. Paraquat shows characteristic peaks at 3055 and 3018 cm^{-1}, assigned to the C–H tension mode of the methyl groups on the aromatic ring in the paraquat molecule; and a set of bands between 1641 and 1194 cm^{-1} assigned to the C–C tension mode and the C–H deformation mode in the aromatic ring plane [46]. Silica peaks are observed in the IR spectra of PQ^{2+}–SiO_2 although the shoulder at 1364 cm^{-1} disappears and new peaks are located at 1647, 1507, 1458 and 557 cm^{-1} related to the binding between the herbicide and the solid. This binding generates binary surface species SiO_2–PQ^{2+}, whose formation is mainly driven by electrostatic interactions, where negatively charged groups of silica could bind the dication by forming ionic pairs or outer-sphere complexes.

The effects of ionic strength (KCl concentration) on the adsorption of PQ^{2+} isotherms on SiO_2 at pH 9.5 and 25 °C are shown in Fig. 6. The adsorption on SiO_2 depends on the presence of electrolyte, decreasing as KCl concentration increases. Even though the effect is not very strong, the results suggest that formation of outer-sphere complexes (or ionic pairs) is taking place on SiO_2, and competition between PQ^{2+} and K^+ for negatively charged groups occurs, leading to a decrease in pesticide adsorption by

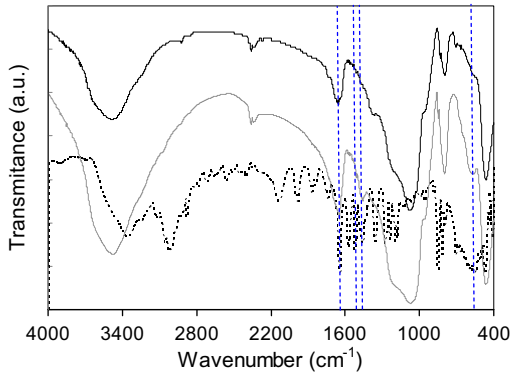

Fig. 5. FTIR spectra of: SiO_2 (black line), PQ^{2+} (dotted line), and PQ^{2+}-SiO_2 (grey line).

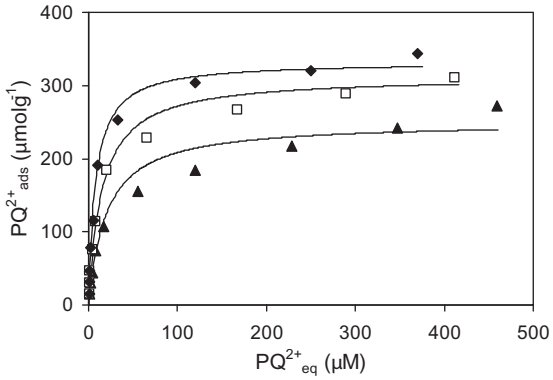

Fig. 6. Effect of KCl concentration on the adsorption of PQ^{2+} on SiO_2 at pH 9.5 and 25 °C. KCl concentrations: diamonds, 0 M; squares, 0.03 M; and triangles, 0.10 M. Lines show predictions of Eq. (3).

increasing K^+ concentration. The results resemble those reported by Tsai et al. [25] for the adsorption of PQ^{2+} on activated clays, where competition between PQ^{2+} and electrolyte cations was proposed to play a key role.

The effects of temperature on the adsorption of PQ^{2+} on SiO_2 at pH 9.5 are shown in Fig. 7. The adsorption on SiO_2 depends on the temperature, decreasing as temperature increases from 5 °C to 45 °C. The negative dependence of the adsorption of PQ^{2+} with the temperature is consistent with formation of outer-sphere complexes or ionic pairs, where there is competition with the cations of the supporting electrolyte. Similar results were reported by Nakamura et al. [47] on the adsorption of PQ^{2+} on activated carbon.

In Figs. 4, 6 and 7 symbols correspond to data points whereas solid lines correspond to the best-fitting Langmuir isotherms calculated by adjusting the parameters q_{mon} and K_L. These parameters are listed in Table 2. Even though the formulated model is rather

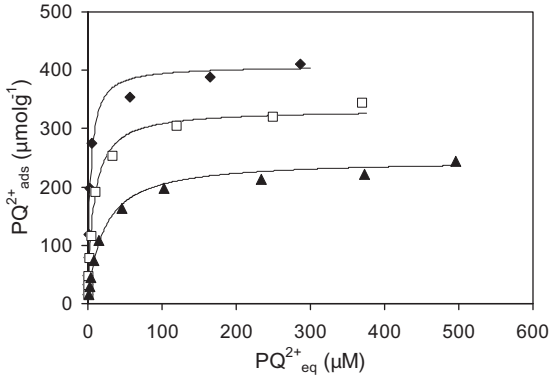

Fig. 7. Effect of temperature on the adsorption of PQ^{2+} on SiO_2 at pH 9.5. Temperatures: diamonds, 5 °C; squares, 25 °C; and triangles, 45 °C. Lines show predictions of Eq. (3).

Table 2
Langmuir model parameters for PQ^{2+} adsorption on SiO_2.

pH	T (°C)	I (M)	K_L (L μmol^{-1})	$q_{mon} \times 10^3$ (μmol g^{-1})	r^2
4.4	25	0.00	100.0	0.26	0.99
7.0	25	0.00	135.1	1.09	1.00
9.5	25	0.00	322.6	12.76	1.00
9.5	5	0.00	408.2	29.52	1.00
9.5	45	0.00	246.9	5.04	1.00
9.5	25	0.03	312.5	6.65	0.99
9.5	25	0.10	250.0	4.98	1.00

simple, it can fit reasonably well the adsorption of PQ^{2+}, i.e., the goodness-of-fit of Eq. (3) was checked through the r^2 values, which was between 0.99 and 1 in all cases. The last result is expected mainly because the Langmuir's theory assumes monolayer coverage of adsorbate over a homogenous adsorbent surface [32]. On the one hand, changes in pH and ionic strength result in important changes in the adsorption isotherm, i.e., q_{mon} and K_L increase as pH increases or ionic strength and temperature decrease. On the other hand, the maximum adsorption capacity (q_{max}) on SiO_2 is 416 μmol g^{-1}, that is favorably compared with those using natural (or synthetic) adsorbents for removal PQ^{2+}, as shown in Table 3 [16,17,19,24,25,43,44,48–59]. In fact, this table shows two adsorbents with higher adsorption capacity than the SiO_2 synthesized in this work, e.g. a humic acid (HA) and a rice husk modified with methacrylic acid. However, the HA particles are not suitable as adsorbent due to their dissolution in aqueous solution [60], and the use of methacrylic acid is still questionable due to its high toxicity [61]. Additionally, the differences in q_{max} between SBA-15 and MCM-41 could be attributed to the fact that the synthesis conditions, e.g. pH and type and concentration of surfactant/s used as template, play an important role on the morphology and reactivity of active sites of silica [20]. Thus, the present results indicate that mesoporous silica with MCM-41 type structure can act as a good and potential adsorbent for PQ^{2+} (and probably for other ionic pollutants).

From the data showed in Fig. 7 the thermodynamic parameters Gibbs free energy ($\Delta G°$), enthalpy ($\Delta H°$), and entropy ($\Delta S°$) for the adsorption of PQ^{2+} on the studied materials can be also obtained by using the following equations:

$$\Delta G^{\circ} = -RT \ln K \quad (6)$$

$$\ln K = \frac{\Delta S^{\circ}}{R} - \frac{\Delta H^{\circ}}{RT} \quad (7)$$

where K is the equilibrium constant, T is the absolute temperature, and R is the gas constant (8.314 J K^{-1} mol^{-1}). The Langmuir isotherm can be applied to calculate the thermodynamic parameters assuming that $K = K_L$. $\Delta H°$ is obtained from van't Hoff plots as ln K_L versus $1/T$. The thermodynamic parameters are shown in Table 4. Physisorption and chemisorption are sometimes classified by the magnitude of the enthalpy change. When $\Delta H°$ is in the range of (0–10) kJ mol^{-1}, the adsorption mechanism is considered to be physisorption; i.e., the bond between adsorbent and adsorbate is due to van der Waals interactions. When $\Delta H°$ is in the range of (30–70) kJ mol^{-1}, the adsorption is considered to be chemisorption; i.e., a chemical bond is formed between the adsorbate and the surface [62]. However, the above classification is commonly used to interpret adsorption at the solid–gas interface, which may significantly differ from the solid–liquid interface. In this last case, if a ligand or ion exchange reaction takes place between the adsorbate and the functional groups of the surface the $\Delta H°$ values could be negative, positive or even zero (with magnitudes up to 70 kJ mol^{-1}) and still be a chemisorption reaction [63,64]. The $\Delta H°$ value for the adsorption of PQ^{2+} on SiO_2 is negative implying that the interaction of the pesticide with the solid is an exothermic process. The negative sorption entropy indicates a decreased randomness at the solid–water interface during PQ^{2+} adsorption [65]. Finally, the negative value of $\Delta G°$ at various temperatures shows that the nature of adsorption on SiO_2 is spontaneous under standard conditions.

Table 3
Maximum adsorption capacities for several natural (and synthetic) adsorbents.

Adsorbent	q_{max} (μmol g^{-1})	Refs.
Activated carbon	295	[48]
Humic acid (HA)	840	[44]
Fulvic acid	390	[44]
Soil organic matter	200	[49]
HA–goethite	43.1	[24]
Iron oxide–quartz	1.9	[50]
Diatomaceous earth	68.2	[25]
Activated bleaching earth	154	[51]
Polyacrimide/methylcellulose hydrogels	55.6	[52]
Methacrylic acid modified rice husk	1137	[53]
Biopolymeric membranes	31.7–77.8	[54]
Illite	41–72.3	[55,56]
Sepiolote	8.6	[43]
Kaolinite	20	[55]
Bentonite	432	[57]
Organoclays	38–223	[58]
Tropical soils	29.2	[59]
Phillipsite–faujasite	18.2–27.2	[16]
Modified zeolite Y	270	[17]
SBA-15 SiO2	214	[19]
MCM-41 SiO2	416	This work

Table 4
Thermodynamic parameters for PQ^{2+} adsorption on the studied material.

T (°C)	$\Delta G°$ (kJ mol^{-1})	$\Delta H°$ (kJ mol^{-1})	$\Delta S°$ (J K^{-1} mol^{-1})
5	−29.11		
25	−29.13	−32.38	−11.49
45	−28.62		

3.3. Recycling of the adsorbent

To study the feasibility and practical potential of synthetized MCM-41 as adsorbent, it was necessary to study the regeneration and reusability of the solid. As a consequence, the removal efficiency in each cycle is shown in Fig. 8. When the material is successively washed with a 0.2 M HCl solution, the removal efficiency is more than 75% after being used four times. Similar results were reported by Yang et al. [66] on the adsorption of aniline on surface-modified MCM-41. Additionally, Mureseanu et al. [67] reported, by using XRD and FTIR spectroscopy, that the structure of the silica was not altered after 3-times regeneration by acid treatment. On the other hand, when the solid is subsequently washed with only water the removal efficiency is around 30% suggesting that protonation of functional surface groups on SiO_2 (mainly hydroxyl groups), induced by acid washing, enhances the desorption of the pesticide [68]. Moreover, the narrow mesopore channels, as shown in Fig. 1c and d, can hinder the transport of the PQ^{2+} ions between the inner and outer of mesoporous silica shell (i.e., the pore size of the material is close to microporosity), so that the pesticide molecules are always clogged in the pore channels and

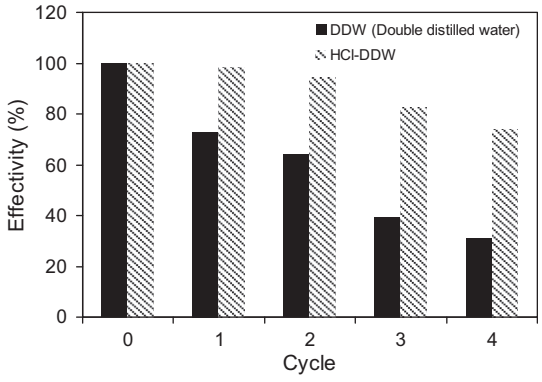

Fig. 8. PQ^{2+} adsorption capacity of SiO_2 after regeneration and reuse cycles at 25 °C. Regeneration solvents: black bars, water; and hatched bars, HCl–water.

difficult to be released [68]. This obstruction seems to play also a key role in the decrease of removal efficiency of PQ^{2+} by the solid regenerated by acid washing.

4. Conclusions

The results shown in this article reveal that the adsorption of PQ^{2+} on mesoporous silica with a MCM-41 type structure is fast and strongly dependent on pH, increasing as pH decreases. The adsorption of PQ^{2+} on SiO_2 is believed to be related to electrostatic attractions and outer sphere complexes (or ionic pairs) formations between the functional groups of the pesticide and the silica active sites, as deduced from adsorption experiments performed at different ionic strengths and temperatures. The maximum adsorption capacity is 416 μmol g^{-1}, which is favourably compared with soils and soils components used for those proposes. Regeneration studies show that the acid washing strongly increases the reusability of the SiO_2 (after 4 cycles) in comparison with using water as extracting agent. Finally, the analysis of thermodynamic parameters suggests that the adsorption on the studied material is exothermic and spontaneous under standard conditions.

The present results demonstrate that the highly-ordered mesoporous silicas are promising candidates for removing herbicides (and other ionic pollutants) from aqueous solutions in environmental and engineering applications.

Acknowledgements

This work was financed by SECyT-UNS, CONICET and ANPCyT. M.B. and M.A. are members of CONICET. The authors thank M.A. Volpe (PLAPIQUI-CONICET) for helpful comments.

References

[1] S.H. Kim, H.H. Ngo, H.K. Shon, S. Vigneswaran, Sep. Purif. Technol. 58 (2008) 335–342.
[2] W. Amondham, P. Parkpian, C. Polprasert, R.D. Delaune, A. Jugsujinda, J. Environ. Sci. Health B 41 (2006) 485–507.
[3] F. Sannino, S. Ruocco, A. Marocco, S. Esposito, M. Pansini, J. Hazard. Mater. 229–230 (2012) 354–360.
[4] R.H. Bromilow, Pest Manage. Sci. 60 (2004) 340–349.
[5] M.S.F. Santos, G. Schaule, A. Alves, L.M. Madeira, Chem. Eng. J. 229 (2013) 324–333.
[6] L.L. Smith, Hum. Exp. Toxicol. 6 (1987) 31–36.
[7] H.J. Beckie, Pest Manage. Sci. 67 (2011) 1037–1048.
[8] R.J. Dinis-Oliveira, F. Remião, H. Carmo, J.A. Duarte, A. Sanchez Navarro, M.L. Bastos, F. Carvalho, Neurotoxicology 27 (2006) 1110–1122.
[9] N.A. Buckley, L. Karalliedde, A. Dawson, N. Senanayake, M. Eddleston, Clin. Toxicol. 42 (2004) 113–116.
[10] C.T. Kresge, M.E. Leonowicz, W.J. Roth, J.C. Vartuli, J.S. Breck, Nature 359 (1992) 710–712.
[11] Z.A. AlOthman, A.W. Apblett, Appl. Surf. Sci. 256 (2010) 3573–3580.
[12] A. Vinu, M. Hartmann, Stud. Surf. Sci. Catal. 154 (2004) 2987–2994.
[13] M. Mesa, L. Sierra, J.L. Guth, Microporous Mesoporous Mater. 102 (2007) 70–79.
[14] Z. Chen, X. Li, H. He, Z. Ren, Y. Liu, J. Wang, Z. Li, G. Shen, G. Han, Colloid Surf. B 95 (2012) 274–278.
[15] R.K.S. Almeida, C.T.G.V.M.T. Pires, C. Airoldi, Chem. Eng. J. 203 (2012) 36–42.
[16] K.M. Ibrahim, H.A. Jbara, J. Hazard. Mater. 163 (2009) 82–86.
[17] H. Zhang, Y. Kim, P.K. Dutta, Microporous Mesoporous Mater. 88 (2006) 312–318.
[18] W. Rongchapo, O. Sophiphun, K. Rintramee, S. Prayoonpokarach, J. Wittayakun, Water Sci. Technol. 68 (2013) 863–869.
[19] F.K. Shieh, C.T. Hsiao, J.W. Wu, Y.C. Sue, Y.L. Bao, Y.H. Liu, L. Wan, M.H. Hsu, J.R. Deka, H.M. Kao, J. Hazard. Mater. 260 (2013) 1083–1091.
[20] M. Brigante, P. Schulz, J. Colloid Interface Sci. 369 (2012) 71–81.
[21] P. Leroy, C. Tournassat, M. Bizi, J. Colloid Interface Sci. 356 (2011) 442–453.
[22] S. Azizian, J. Colloid Interface Sci. 276 (2004) 47–52.
[23] C.E. Zubieta, P.V. Messina, C. Luengo, M. Dennehy, O. Pieroni, P.C. Schulz, J. Hazard. Mater. 152 (2008) 765–777.
[24] M. Brigante, G. Zanini, M. Avena, J. Hazard. Mater. 184 (2010) 241–247.
[25] W.T. Tsai, K.J. Hsien, Y.M. Chang, C.C. Lo, Bioresour. Technol. 96 (2005) 657–663.
[26] K. Zhang, H.L. Chen, B. Albela, J.G. Jiang, Y.M. Wang, M.Y. He, L. Bonneviot, Eur. J. Inorg. Chem. 2011 (2011) 59–67.
[27] K. Zhang, E.H. Yuan, L.L. Xu, Q.S. Xue, C. Luo, B. Albela, L. Bonneviot, Eur. J. Inorg. Chem. 2012 (2012) 4183–4189.
[28] G.S. Park, C.W. Ahn, M.W. Kim, J. Am. Ceram. Soc. 85 (2002) 2542–2544.
[29] M. Mesa, L. Sierra, J.L. Guth, Microporous Mesoporous Mater. 112 (2008) 338–350.
[30] C.J. Brinker, G.W. Scherer, Sol–Gel Science, Academic Press, San Diego, 1990.
[31] L. Qi, J. Ma, H. Cheng, Z. Zhao, Chem. Mater. 10 (1998) 1623–1626.
[32] M. Brigante, P. Schulz, J. Hazard. Mater. 192 (2011) 1597–1608.
[33] G. Gu, P.P. Ong, C. Chu, J. Phys. Chem. Solids 60 (1999) 943–947.
[34] B. Dou, Q. Hu, J. Li, S. Qiao, Z. Hao, J. Hazard. Mater. 186 (2011) 1615–1624.
[35] P.I. Ravikovitch, D. Wei, W.T. Chueh, G.L. Haller, A.V. Neimark, J. Phys. Chem. B 101 (1997) 3671–3679.
[36] M. Kruk, M. Jaroniec, Y. Sakamoto, O. Terasaki, R. Ryoo, C.H. Ko, J. Phys. Chem. B 104 (2000) 292–301.
[37] K. Gude, V.M. Gun'ko, J.P. Blitz, Colloid Surf. A 325 (2008) 17–20.
[38] M. Kosmulski, J. Colloid Interface Sci. 353 (2011) 1–15.
[39] M. Brigante, P. Schulz, J. Colloid Interface Sci. 363 (2011) 355–361.
[40] W.C. Chang, J.R. Deka, H.Y. Wu, F.K. Shieh, S.Y. Huang, H.M. Kao, Appl. Catal. B 142–143 (2013) 817–827.
[41] T.X. Bui, V.H. Pham, S.T. Le, H. Choi, J. Hazard. Mater. 254–255 (2013) 345–353.
[42] W.H. Cheung, Y.S. Szeto, G. McKay, Bioresour. Technol. 98 (2007) 2897–2904.
[43] G. Rytwo, S. Nir, L. Margulies, Soil Sci. Soc. Am. J. 60 (1996) 601–610.
[44] A. Iglesias, R. López, D. Gondar, J. Antelo, S. Fiol, F. Arce, Chemosphere 76 (2009) 107–113.
[45] D.L. Sparks, Environmental Soil Chemistry, Academic Press, San Diego, CA, USA, 1995.
[46] E. González-Pradas, M. Villafranca-Sánchez, F. Del Rey-Bueno, M.D. Ureña-Amate, M. Fernández-Pérez, Pest Manage. Sci. 56 (2000) 565–570.
[47] T. Nakamura, N. Kawasaki, H. Ogawa, S. Tanada, M. Kogirima, M. Imaki, Toxicol. Environ. Chem. 70 (1999) 275–280.
[48] N.K. Hamadi, S. Swaminathan, X.D. Chen, J. Hazard. Mater. 112 (2004) 133–141.
[49] D. Gondar, R. López, J. Antelo, S. Fiol, F. Arce, J. Hazard. Mater. 235–236 (2012) 218–223.
[50] M. Pateiro-Moure, A. Bermúdez-Couso, D. Fernández-Calviño, M. Arias-Estévez, R. Rial-Otero, J. Simal-Gándara, J. Chem. Eng. Data 55 (2010) 2668–2672.
[51] W.T. Tsai, C.W. Lai, K.J. Hsien, Chemosphere 55 (2004) 829–837.
[52] F.A. Aouada, Z. Pan, W.J. Orts, H.C.L. Mattoso, J. Appl. Polym. Sci. 114 (2009) 2139–2148.
[53] S.T. Hsu, L.C. Chen, C.C. Lee, T.C. Pan, B.X. You, Q.F. Yan, J. Hazard. Mater. 171 (2009) 465–470.
[54] D.S. Cocenza, M.A. De Moraes, M.M. Beppu, L.F. Fraceto, Water Air Soil Pollut. 223 (2012) 3093–3104.
[55] A. Keizer, Prog. Colloid Polym. Sci. 83 (1990) 118–126.
[56] W.T. Tsai, C.W. Lai, J. Hazard. Mater. 134 (2006) 144–148.
[57] D. Ait Sidhoum, M.M. Socías-Viciana, M.D. Ureña-Amate, A. Derdour, E. González-Pradas, N. Debbagh-Boutarbouch, Appl. Clay Sci. 83–84 (2013) 441–448.
[58] Y. Seki, K. Yurdakoç, J. Colloid Interface Sci. 287 (2005) 1–5.
[59] A.S.R. Juo, O.O. Oginni, J. Environ. Qual. 7 (1978) 9–12.
[60] M. Brigante, G. Zanini, M. Avena, Colloid Surf. A 294 (2007) 64–70.
[61] A.M. Saillenfait, P. Bonnet, F. Gallissot, A. Peltier, J.F. Fabriès, Toxicol. Sci. 50 (1999) 136–145.
[62] F. Chen, C. Zhou, G. Li, F. Peng, Arabian J. Chem. (in press). doi: http://dx.doi.org/10.1016/j.arabjc.2012.04.014.
[63] D.P. Rodda, B.B. Johnson, J.D. Wells, J. Colloid Interface Sci. 184 (1996) 365–377.
[64] G. Sposito, The Surface Chemistry of Natural Particles, Oxford University Press, New York, USA, 2004.
[65] E. Tanis, K. Hanna, E. Emmanuel, Colloid Surf. A 327 (2008) 57–63.
[66] X. Yang, Q. Guan, W. Li, J. Environ. Manage. 92 (2011) 2939–2943.
[67] M. Mureseanu, A. Reiss, I. Stefanescu, E. David, V. Parvulescu, G. Renard, V. Hulea, Chemosphere 73 (2008) 1499–1504.
[68] X. Fu, X. Chen, J. Wang, J. Liu, Microporous Mesoporous Mater. 139 (2011) 8–15.